Environmental Science and Engineering

Long Quoc Nguyen
Luyen Khac Bui
Xuan-Nam Bui
Hai Thanh Tran *Editors*

Advances in Geospatial Technology in Mining and Earth Sciences

Selected Papers of the 2nd International Conference on Geo-spatial Technologies and Earth Resources 2022

Springer

Long Quoc Nguyen · Luyen Khac Bui ·
Xuan-Nam Bui · Hai Thanh Tran
Editors

Advances in Geospatial Technology in Mining and Earth Sciences

Selected Papers of the 2nd International Conference on Geo-spatial Technologies and Earth Resources 2022

Springer

Contents

Application of Unmanned Aerial Vehicles for Surveying and Mapping in Mines: A Review 1
Long Quoc Nguyen, Minh Tuyet Dang, Luyen K. Bui, Quy Bui Ngoc, and Truong Xuan Tran

Mining-Induced Land Subsidence Detected by Persistent Scatterer InSAR: Case Study in Pniówek Coal Mine, Silesian Voivodeship, Poland 23
Thi Thu Huong Kim, Hong Ha Tran, Tuan Anh Phan, and Tomasz Lipecki

Slope Stability Evaluation of Fenghuangshan Landfill Under Rainfall Condition: A Case Study 43
Yuru Chen, Jun Kuang, Renmin Zhu, Jianlin Cao, Jun Zhou, and Qiang Tang

Forecasting PM10 Concentration from Blasting Operations in Open-Pit Mines Using Unmanned Aerial Vehicles and Adaptive Neuro-Fuzzy Inference System 59
Xuan-Nam Bui, Chang Woo Lee, and Hoang Nguyen

Assessing the Effect of Open-Pit Mining Activities and Urbanization on Fine Particulate Matter Concentration by Using Remote Sensing Imagery: A Case Study in Binh Duong Province, Vietnam 75
Thanh Dong Khuc, Long Quoc Nguyen, Dinh Trong Tran, Van Anh Tran, Quynh Nga Nguyen, Xuan Quang Truong, and Hien Quang Pham

Effect of Loading Frequency on the Liquefaction Resistance of Poorly Graded Sand 95
Sung- Sik Park, Dong- Kiem -Lam Tran, Tan-No Nguyen, Seung-Wook Woo, and Hee -Young Sung

An Automatic Method for Clay Minerals Extraction from Landsat 8 OLI Data. A Case Study in Chi Linh City, Hai Duong Province 105
Trinh Le Hung, Nguyen Sach Thanh, and Vuong Trong Kha

Evaluation of the Precision of SARAL/AltiKa and Sentinel-3A Satellite Altimetry Data Over the Vietnam Sea and Its Surroundings ... 121
Do Van Mong, Nguyen Van Sang, Khuong Van Long, and Luyen K. Bui

Detection of GNSS-TEC Noise Related to the Tonga Volcanic Eruption Using Optimization Machine Learning Techniques and Integrated Data 137
Nhung Le, Benjamin Männel, Luyen K. Bui, Mihaela Jarema, Thai Chinh Nguyen, and Harald Schuh

Stability of Road Embankments on Weak Soils 159
Rafail Rafailov

Indirect Georeferencing in Terrestrial Laser Scanning: One-Step and Two-Step Approaches 171
Dung Trung Pham, Long Quoc Nguyen, Tinh Duc Le, and Ha Thanh Tran

Technological Solutions for Fly Ash and Red Mud Upcycling Approach the Vietnam's Government Target of Net-Zero Carbon by 2050 187
Van-Duc Nguyen, Chang-Woo Lee, Xuan-Nam Bui, Pham Van Chung, Quang-Tuan Lai, Hoang Nguyen, Tran Thi Huong Hue, Van-Trieu Do, and Ji-Whan Ahn

Pile–Soil Interaction Mechanism and Optimization Measures Based on Finite Element Method 209
Qi Xu, Remin Zhu, Jianlin Cao, Xuedong Li, Yi Zhang, and Qiang Tang

Determination of Illegal Signs of Coal Mining Expansion in Thai Nguyen Province, Vietnam from a Combination of Radar and Optical Imagery 225
Tran Van Anh, Tran Hong Hanh, Nguyen Quynh Nga, Le Thanh Nghi, Truong Xuan Quang, Khuc Thanh Dong, and Tran Trung Anh

Evaluation of Coal Reserve Reliability in the Nui Beo Mine, Quang Ninh Province Based on the Statistical and Stable Random Function Methods 243
Khuong The Hung, Vu Thai Linh, Pham Thanh Tinh, and Nguyen Khac Duc

Chromite Ore Modeling Based on Detailed Gravity Method in Pursat, Cambodia 259
Trong Cao Dinh, Hung Pham Nam, Thanh Duong Van, Luc Nguyen Manh, Bach Mai Xuan, Trieu Cao Dinh, and Hung Luu Viet

Relationship Between Shear Wave Velocity and Soil Depth and Evaluation of Soil Liquefaction in Quaternary Sedimentary Layer 277
Yu Zhou, Xuedong Li, Yi Zhang, Yibin Li, Xiaoyong Zhang, and Qiang Tang

Characterization of the Natural Dolomite from Thanh Liem Area, Vietnam, and Its Applications 291
Nguyen Thi Thanh Thao, Le Thi Duyen, and Phenglilern Sensousit

A Mine Production Tracking Platform and Its Initial Application in the Digital Transformation for a Vietnamese Coal Exploitation Company 303
Dinh-Van Nguyen, Trung-Kien Dao, Viet-Tung Nguyen, Cong-Dinh Dinh, Trung-Kien Nguyen, Nguyen Quynh Nga, and Chu Thi Khanh Ly

Shear Strength of Poorly Graded Granular Material in Multi-Stage Direct Shear Test 315
Sung-Sik Park, Tan-No Nguyen, Dong-Kiem-Lam Tran, Keum-Bee Hwang, and Hee-Young Sung

High-Resolution Seismic Reflection Survey of Young Sediment at Can Gio Coast, Ho Chi Minh City, Vietnam 325
Thuan Van Nguyen, Cuong Van Anh Le, and Man Ba Duong

Analysis of Geological Structures by 2D Magnetotelluric Inversion in Bang Hot Spring Area, Quang Binh Province 339
Cuong Van Anh Le, Duy Thong Kieu, Ngoc Dat Pham, and Hop Phong Lai

Physicochemical Characteristics of the Middle Triassic Limestone in Ha Nam Province, Vietnam and the Ability of Adsorption of Heavy Metal Ions from Aqueous Environments 357
Bui Hoang Bac, Le Thi Duyen, Nguyen Thi Thanh Thao, and Nguyen Huu Tho

Local Mechanical Behaviors of Steel Box Girder During Skew Incremental Launching 371
Jiabao Du, Wen Niu, Yu Shi, Yongzhe Wu, Yuan Chen, and Qiang Tang

GIS Applications in Land Adaptability Mapping for Perennial Industrial Crops in Nghe An Province, Vietnam 383
Hanh Thi Tong, Kien-Trinh Thi Bui, Cuong Manh Nguyen, and Yit Chanthol

Land-Use and Land-Cover Change Detection and Classification to Analyze Dynamics of Dragon Fruit Farming in Sand Dunes Area of Binh Thuan Province of Vietnam 405
Luan Hong Pham, Trong Dieu Hien Le, Lien T. H. Pham, Ho Nguyen, and Hong Quan Nguyen

Random Forest Analysis of Land Use and Land Cover Change Using Sentinel-2 Data in Van Yen, Yen Bai Province, Vietnam 429
Xuan Quang Truong, Nguyen Hien Duong Dang, Thi Hang Do, Nhat Duong Tran, Thi Thu Nga Do, Van Anh Tran, Vasil Yordanov, Maria Antonia Brovelli, and Thanh Dong Khuc

Engineering Geological Problems of Foundation Pit Construction in Quaternary Strata: Taking Suzhou Area as an Example 447
Xinyu Luo, Peng Yin, Yongsheng Zheng, Xuedong Li, Yi Zhang, and Qiang Tang

Roof Condition Characteristics Affecting the Stability of Coal Pillars and Retained Roadway 463
Quang Phuc Le and Van Chi Dao

On the Flow Assurance for Un-Insulated Subsea Pipeline Systems: Application on the Multiphase Pipeline from Pearl Field to FPSO Ruby II Offshore Vietnam 479
Van Thinh Nguyen, Thi Hai Yen Nguyen, Sylvain S. Guillou, Thuy Huong Duong, Thi Thanh Thuy Truong, and Thi Thao Nguyen

Detection of Underground Anomalies by Evaluation of Ground Penetrating Radar Attribute Combination 495
Duy Hoang Dang, Cuong Van Anh Le, and Thuan Van Nguyen

Dynamic Failure Process of Soil Particles at the End of Shield Tunnel Based on Discrete Element 509
Zheyuan Feng, Bin Liu, Sijun Zhang, Fei Kang, Haipeng Hui, and Qiang Tang

Early Triassic Tectonic Evolution of the Northeastern Kontum Massif: New Constraints from the S-type Granite in Ba To Area, Quang Ngai Province, Central Vietnam 521
Hai Thanh Tran, Bui Vinh Hau, Ngo Xuan Thanh, Nguyen Huu Hiep, and Ngo Thi Kim Chi

Proposal of Study on InSAR-Based Land Subsidence Analysis as Basis for Subsequent Hydro-mechanical Modeling: A Case Study of Hanoi, Vietnam 535
Hong Ha Tran, Luyen K. Bui, Hung Q. Ha, Thi Thu Huong Kim, and Christoph Butscher

An Automatic Method for Clay Minerals Extraction from Landsat 8 OLI Data. A Case Study in Chi Linh City, Hai Duong Province

Trinh Le Hung, Nguyen Sach Thanh, and Vuong Trong Kha

Abstract Landsat satellite data have been effectively used for mineral resources extraction. This paper presents an automatic method for clay minerals extraction from Landsat 8 OLI image based on band rationing and principal component analysis methods. Firstly, the Landsat 8 data is used to calculate the NIR/RED (band5/band4) and SWIR1/SWIR2 (band6/band7) band rationing images. To highlight the distribution of clay minerals, these band rationing images are further used to multiply the digital number values of NIR and SWIR2 bands, then obtaining (band5/4) × band5 and (band6/7) × band7 images. Finally, the principal component analysis (PCA) method is used to calculate the principal components, then select the 2nd principal component (PC2) to detect clay minerals by the automatic thresholding method. The results in this research can be used to provide input information for mineral exploration.

Keywords Remote sensing · Clay minerals · Band rationing · Principal component analysis · Landsat 8 · Chi Linh city

1 Introduction

Located in Southeast Asia, Vietnam is rich in mineral resources, possessing some 60 kinds, making it the seventh ranking country in the top 15 of basic resource countries. Vietnam's main mineral resources consist of coal, phosphates, rare earth elements, bauxite, chromate, copper, gold, iron, manganese, silver, zinc, offshore oil, and gas

T. Le Hung (✉) · N. S. Thanh
Le Quy Don Technical University, Hanoi, Vietnam
e-mail: trinhlehung@lqdtu.edu.vn

N. S. Thanh
e-mail: thanhns.geo@lqdtu.edu.vn

V. T. Kha
Hanoi University of Mining and Geology, Hanoi, Vietnam
e-mail: vuongtrongkha@humg.edu.vn

© The Author(s), under exclusive license to Springer Nature Switzerland AG 2023

L. Q. Nguyen et al. (eds.), *Advances in Geospatial Technology in Mining and Earth Sciences*, Environmental Science and Engineering,
https://doi.org/10.1007/978-3-031-20463-0_7

deposits. Some minerals in Vietnam have important reserves such as bauxite (672.1 million tons), apatite (0.778 million tons), titanium (15.71 million tons), coal (3520 million tons), rare earth (1.1 million tons) and granite (15 billion m^3) [1, 2]. Mineral resources play an important role and have become one of the resources for the socio-economic development of Vietnam. Despite having rich mineral resources, mineral reserves in Vietnam are not large and are being depleted due to the mining process for economic development. Therefore, the exploration and detection of mineral-containing areas is a matter of urgent significance today in Vietnam.

Remote sensing data has been widely used in the world in monitoring and detection of mineral-containing areas [3, 4]. The main remote sensing data in mineral monitoring and detection is multispectral images such as Landsat 5 TM, Landsat 7 ETM+ , Landsat 8 OLI, Aster, and Sentinel 2 MSI [5–9]. Many studies have used these remote sensing images to detect areas containing clay minerals, iron oxide, copper…. [6, 10–12]. Based on the spectral reflectance characteristics of minerals, some techniques have been proposed to detect mineral-containing areas on multi-spectral satellite images such as band rationing method [13, 14], the method based on principal component analysis (PCA), the method based on spectral indices (clay mineral index, iron oxide index, Chica-Olma index, Kaufmann index, Abrams index). Crosta et al. (1989, 1993) used principal component analysis and color composite techniques to detect clay minerals and iron oxides on Landsat TM satellite images [13, 15]. The principal component analysis method and spectral indices are also used in the study of Mia and Fujimitsu (2012), in which the authors used Landsat 7 ETM+ multispectral images for mapping thermal alteration minerals in and around Kuju volcano, Kyushu, Japan [16]. Pour and Hashim (2015) have integrated optical and radar images (PALSAR and ASTER data) for mineral deposits exploration in tropical environments (Central Belt, Peninsular Malaysia) [17].

Fraser and Green (1997) [18] developed DPCA (directed principal component analysis) method for monitoring hydrothermal minerals distribution. The DPCA method is built on the combination of advantages of band rationing and PCA methods, thereby improving the accuracy in detecting exposed minerals from satellite imagery. PCA and DPCA methods are also used in the studies of Trinh et al. [19–21] in some areas of northern Vietnam (Thai Nguyen province, Vinh Phuc province), in which the authors used Landsat TM, Landsat 8 OLI, and Sentinel 2 image data. In their studies, Trinh et al. built the RS-MINERALS computer program based on MATLAB language with tools such as band rationing, principal component analysis, directed principal component analysis for minerals detection and classification from Landsat imagery. The results obtained in these studies show that multispectral image data are effective for detecting areas containing clay and iron minerals, especially areas without vegetation cover [19–21].

The vegetation cover has a great influence on the accuracy of minerals detection results on optical satellite images. Traditional techniques such as band rationing, and principal component analysis methods are highly effective in detecting minerals in areas without vegetation cover. The accuracy of mineral detection from optical satellite images is greatly reduced in areas with vegetation cover. To overcome this

limitation, this study uses a combination of band rationing, principal component analysis methods, and image multiplication technique. The image multiplication technique allows highlighting mineral distribution positions on band rationing images. Meanwhile, the principal component analysis method helps to accurately identify mineral-containing areas on band rationing images. The simultaneous combination of these techniques allows limiting the influence of vegetation cover on mineral detection results from optical satellite images such as Landsat 8 OLI.

The focus of this paper is to propose an automatic method for clay minerals extracting from Landsat 8 OLI multispectral image data. In this study, the red (band 4), near-infrared (band 5), and short-wave infrared bands (band 6 and band 7) Landsat 8 OLI image were used to calculate the band rationing images, and then image multiplication and principal component analysis techniques were used to highlight the clay minerals containing areas. Finally, the automatic thresholding method is used to classify clay minerals containing areas from principal component (PC) images.

2 Study Area and Materials

2.1 Study Area

Chi Linh is a city located in the north of Hai Duong province, Vietnam. The north and northeast of the city are mountainous areas belonging to the Dong Trieu arc, the other three sides are surrounded by Kinh Thay, Thai Binh, and Dong Mai rivers. Chi Linh city has a natural area of 282.91 km, and is the district-level administrative unit with the largest area in Hai Duong province. The population of Chi Linh city in 2018 is about 220,400 people [22].

The terrain of Chi Linh city is diverse with an area of hills, alternating plains, and sloping terrain from the north to the south. North of the city is a mountainous area with natural and planted forests, the highest peak is Day Dieu with a height of 616 m. The southern part of the study area has a flat terrain with alluvial flats [22].

Chi Linh city is located in the tropical monsoon climate with 2 distinct seasons: the dry season from October to April next year and the rainy season from April to September every year. The average annual temperature is 23°C, the average annual rainfall is 1463 mm [22].

Mineral resources in Chi Linh city are not of many types, but some types of minerals have large reserves and economic value such as: Kaolin (reserve of 40000 tons), refractory clay (8 million tons), stone, construction yellow sand, brown coal mine (reserves in billions of tons). Currently, there are dozens of mining sites in Chi Linh city and the mining industry plays an important role in local socio-economic development [22].

The geographical location of Chi Linh city (Hai Duong province) is shown in Fig. 1.

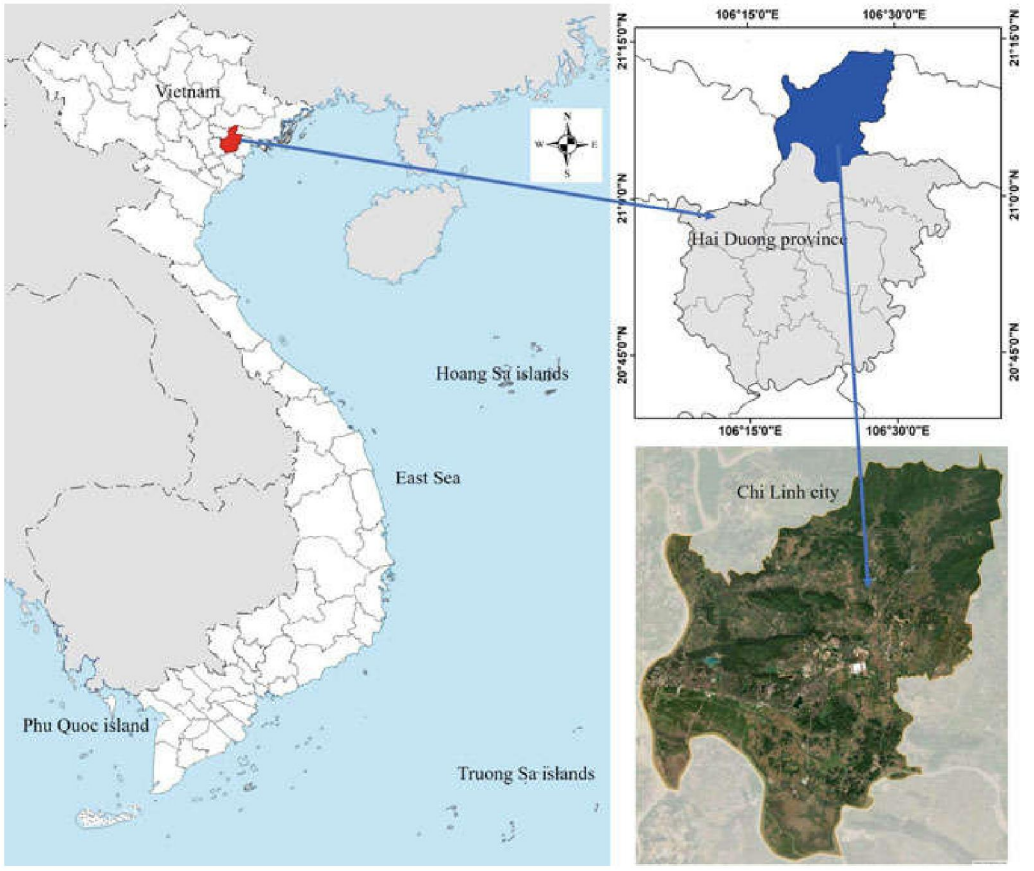

Fig. 1 Study area, Chi Linh city, Hai Duong province

2.2 *Materials*

LANDSAT 8 is the 8th generation satellite of the LANDSAT program (NASA, USA), using 2 sensors: Operational Land Imager (OLI) and Thermal InfraRed (TIRS). LANDSAT 8 was launched into orbit on February 11, 2013. LANDSAT 8 provides images in 11 spectral bands, including 9 multispectral bands with 30 m spatial resolution, 1 panchromatic band with 15 m resolution, and 2 thermal infrared bands at 100 m resolution (Table 1). The temporal resolution of the Landsat 8 image is 16 days, and with the successful launch of the Landsat 9 satellite (September 27, 2021) with completely similar characteristics to the Landsat 8, the temporal resolution of the Landsat 8/9 image is reduced to 8 days. Data from Landsat 9 was publicly available from USGS in early 2022. The shortening of image acquisition process allows improving the efficiency of the application of Landsat 8/9 satellite image data in Earth observation [23, 24].

Until September 2021, Landsat 8 had added 1.86 million images to the archive (about 20% of the total archive holdings) and each day since, Landsat 8 has added another ~ 700 new scenes. Landsat 9, like Landsat 8, is both radiometrically and geometrically better than earlier generation Landsats. Landsat data in the U.S. archive

Table 1 Landsat 8 OLI_TIRS bands characteristics

No	Landsat 8 OLI_TIRS bands	Wavelength (μm)	Resolution (m)
1	Band 1–Coastal/Aerosol	0.433–0.453	30
2	Band 2–Blue	0.450–0.515	30
3	Band 3–Green	0.525–0.600	30
4	Band 4–Red	0.630–0.680	30
5	Band 5–Near Infrared (NIR)	0.845–0.885	30
6	Band 6–Middle Infrared (MIR)	1.560–1.660	30
7	Band 7–Middle Infrared (MIR)	2.100–2.300	30
8	Band 8–Panchromatic (PAN)	0.500–0.680	15
9	Band 9–Cirrus	1.360–1.390	30
10	Band 10–Thermal Infrared (TIR)	10.30–11.30	100
11	Band 11–Thermal Infrared (TIR)	11.50–12.50	100

contributed by each Landsat satellite as of September 30, 2021, is shown in Fig. 2 [23].

In this study, the multispectral cloud-free Landsat 8 OLI image with a spatial resolution of 30 m (multispectral bands) and 100 m (thermal infrared bands), acquired on December 01, 2021, in Chi Linh city (Hai Duong province) was used for extracting clay minerals containing areas. The Landsat 8 data was the L2 level product, downloaded from the United States Geological Survey website (https://glovis.usgs.gov). Landsat 8 Level 2 provides global surface reflectance and surface temperature science

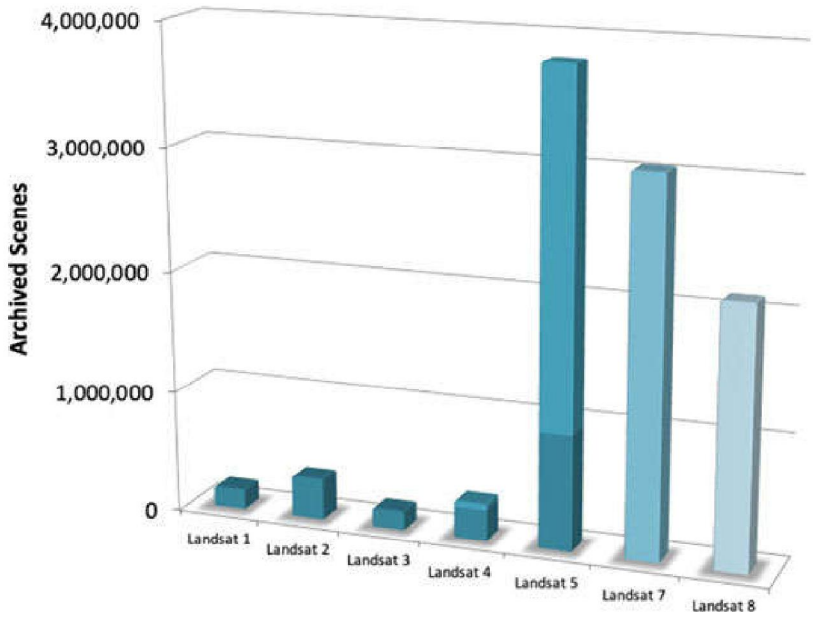

Fig. 2 Landsat data in the U.S. archive contributed by each Landsat satellite as of September 30, 2021 [23]

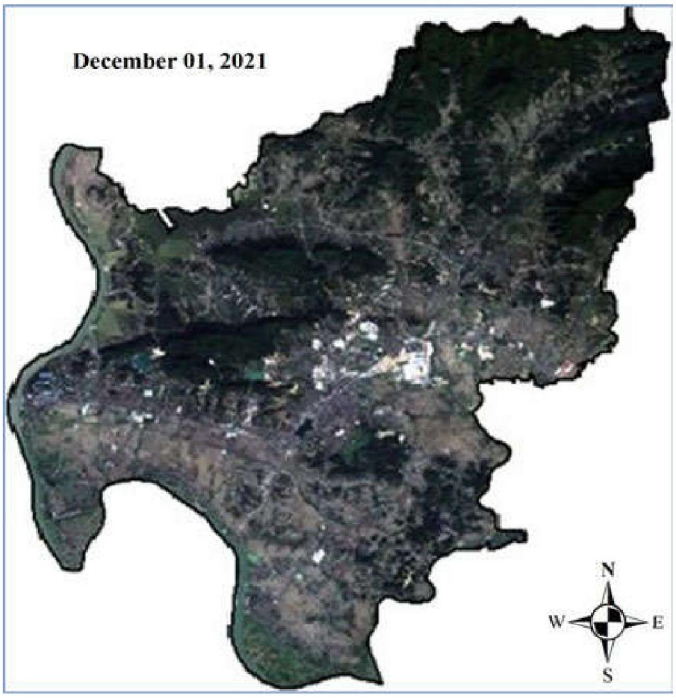

Fig. 3 Landsat 8 multispectral image, December 01, 2021

products. Level 2 science products are generated from Collection 2 Level-1 inputs that meet the < 76 degrees Solar Zenith Angle constraint and include the required auxiliary data inputs to generate a scientifically viable product [24].

Landsat 8 image data used in this study is presented in Fig. 3 (in the natural color band combination with red (band 4), green (band 3), and blue (band 2) bands).

3 Methodology

All studies are based on the difference between the spectral reflectance of minerals and other land cover objects to detect minerals from remote sensing data [25, 26]. Figure 4 shows the reflectance spectra of clay minerals and other hydrothermal alterations (source: Clark et al., 1989; Clark, 1999) [25, 27]. The vertical axis shows the percentage of incident sunlight that is reflected by the materials. The horizontal axis shows the wavelengths of energy for the reflected portion (1.0 to 3.0 μm) of the infrared (IR) region. The spectral reflectance curve shows that the maximum reflectance of iron oxide occurs in band 6 (MIR1, 1.56–1.66 μm) and that reflectance is considerably lower in band 7 (MIR2, 2.10–2.30 μm) LANDSAT 8 OLI multispectral images. Therefore, the band6/band7 rationing image is used to highlight the areas containing clay minerals. To increase the contrast between clay minerals and other land cover objects, this band rationing image is further multiplied by the band 7 digital number values.

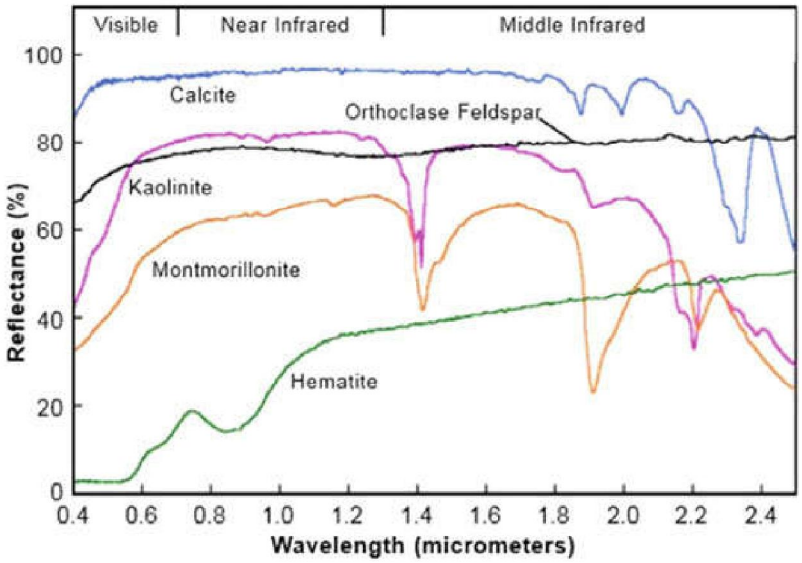

Fig. 4 Spectral reflectance of different clay minerals [25, 27]

On the other hand, vegetation cover absorbs electromagnetic radiation energy in the red spectral band and strongly reflects it in the near infrared spectral band (Fig. 5) [28]. Therefore, to eliminate the influence of vegetation cover on mineral detection results from remote sensing multispectral images, in this study, the band rationing image between near-infrared band (band 5) and red band (band 4) of Landsat 8 OLI data is used. To further increase the contrast between vegetation and other land cover objects, this band rationing image is multiplied by the digital number value of the near-infrared band (band 5), the result is an image (band5/4) × band5.

In the next step, principal components analysis method is used to calculate principal components (PC) from two band rationing images: (band5/4) × band5 and (band6/7) × band7. The PCA method uses the principal components transformation technique for reducing dimensionality of correlated multispectral data [29]. The analysis is based on multivariate statistical technique that selects uncorrelated linear combinations of variables in such a way that each successively extracted linear combination, or PC, has a smaller variance. Eigenvalues give information using magnitude and sign about which spectral properties of vegetation, rocks, and soils are responsible for the statistical variance mapped into each PC [16]. Finally, an automatic thresholding method is used to extract the clay minerals containing areas from PC image. The accuracy of detection areas containing clay minerals is evaluated based on Google high spatial resolution satellite image data and geological maps of the study area. The flowchart for the methodology used in this study to extract shoreline changes based on Landsat multi-temporal data is shown in Fig. 6.

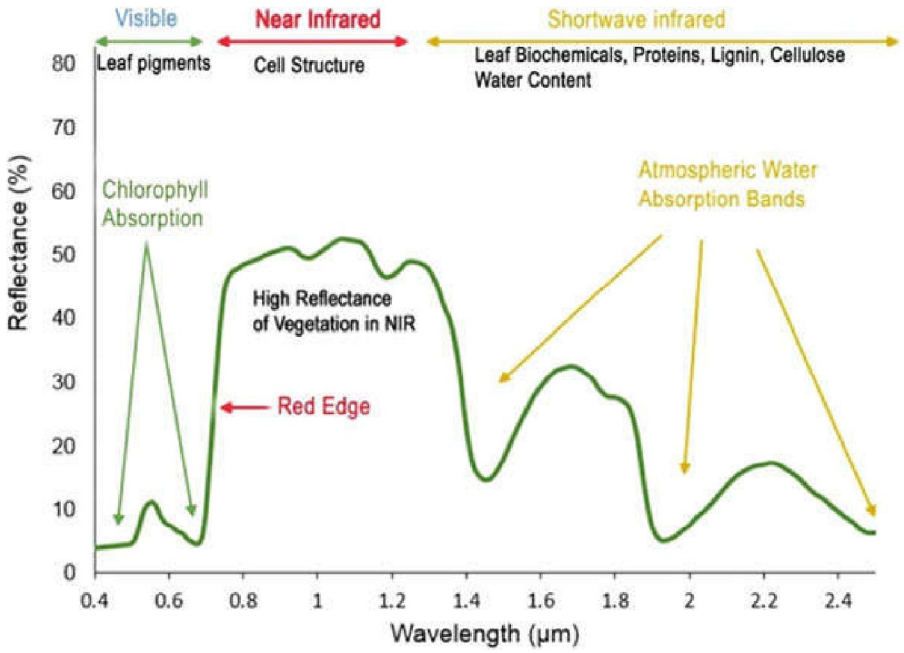

Fig. 5 Spectral characteristics of vegetation cover [28]

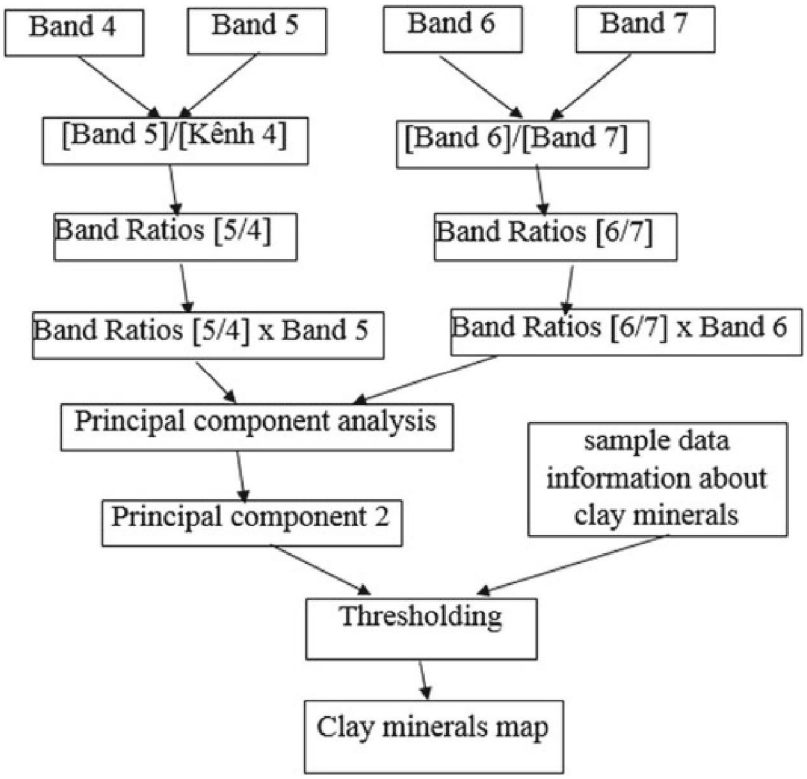

Fig. 6 Flowchart of the methodology for clay minerals extraction from Landsat 8 OLI multispectral data

4 Results and Discussion

Landsat 8 OLI data is collected at the L2A processing level (Bottom of atmosphere reflectance value), so in this study, only geometric correction was carried out to convert to the local coordinate system VN-2000. The red, near infrared and two middle infrared bands of Landsat 8 OLI image taken on December 01, 2021, are used to calculate the band rationing images. The band rationing images: Band5/Band4 and Band6/Band7 calculated from Landsat 8 OLI data in this study are shown in Fig. 7. Vegetation cover is shown in bright white pixels on band5/band4 rationing image due to strong reflection of electromagnetic radiation energy in near infrared band (band 5) and absorption in the red band (band 4) of Landsat 8 OLI image. In band6/band7 band rationing image, clay minerals are represented by bright white and are difficult to distinguish from vegetation cover.

Figure 8 shows images (Band5/4) × Band5 and (Band6/7) × Band6 after using image multiplication technique to better highlight the vegetation cover and clay minerals from band rationing images.

Table 2 shows the eigenvector matrix values and eigenvalues of the PCA for the (Band5/4) × Band5 and (Band6/7) × Band6 images. The analysis of eigenvalues and eigenvectors shows that the first principal component (PC1) contains information about the land surface cover, focusing on the vegetation cover. Meanwhile, the second principal component (PC2) contains information about the distribution of clay minerals. As can be seen, PC1—the "albedo" image, is about 97.405% of eigenvalue of the total variance for unstretched data PCA. PC2 contains 2.595% information of two band rationing images. In this study area, PC2 highlights clay minerals as bright white pixels because of the greatest loading of (Band6/7) × Band6 image (0.965478) and (Band5/4) × Band5 image (−0.260485) (Table 2).

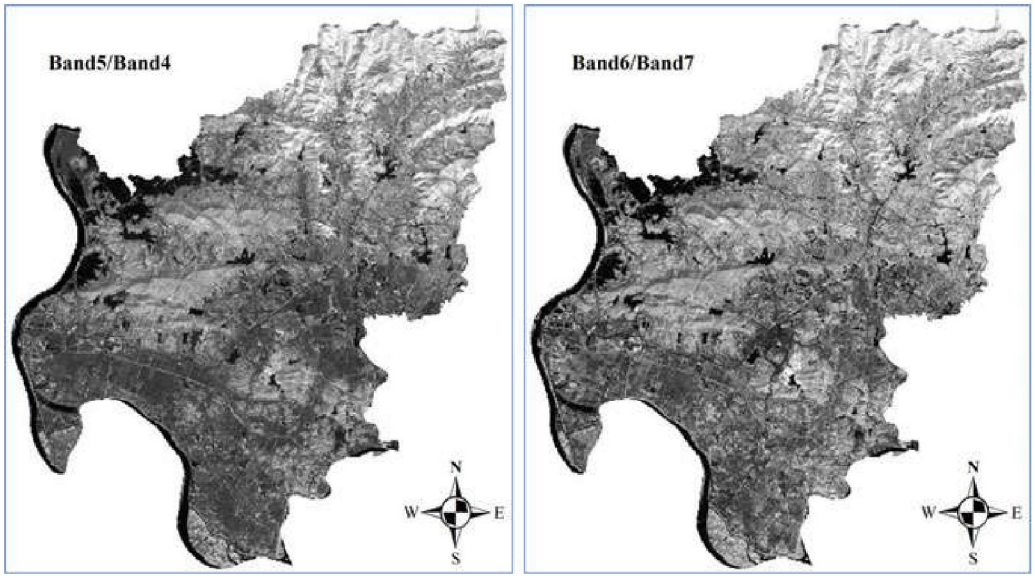

Fig. 7 The band rationing images: Band5/Band4 and Band6/Band7

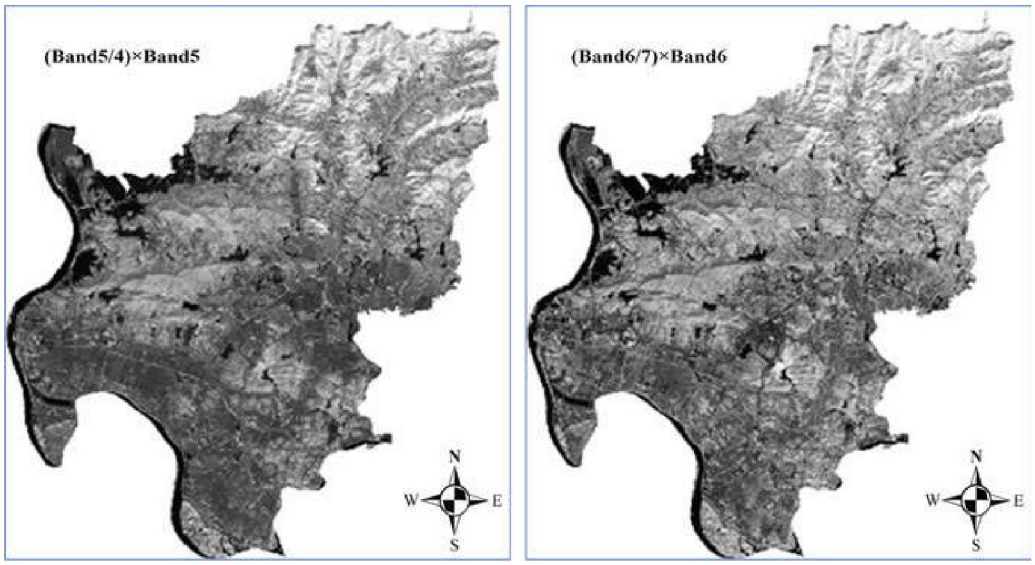

Fig. 8 The band rationing images: (Band5/4) × Band5 and (Band6/7) × Band6

Table 2 The eigenvector matrix values and eigenvalues of the PCA for the (Band5/4) × Band5 and (Band6/7) × Band6 images

Principal component	Eigen matrix		Eigenvalues (%)
	(Band5/4) × Band5	(Band6/7) × Band6	
PC1	0.965478	0.2604845	97.405
PC2	− 0.260485	0.965478	2.595

The two PC transformation on unstretched (Band5/4) × Band5 and (Band6/7) × Band6 images of study area are shown in Fig. 9.

The anomalies for clay minerals containing areas are determined based on a threshold of $\mu + 2^*\sigma$, where μ and σ represent the mean value and standard deviation of the relevant PC images, respectively [7]. Figure 10 shows the final result for clay minerals containing areas derived from Landsat 8 OLI data in Chi Linh city (Hai Duong province), in which the clay minerals containing areas are depicted as red color. The results presented in this figure show that the clay minerals are scattered throughout Chi Linh city, in which the most concentration is in the central region. Large clay mineral deposits in Chi Linh city such as Co Kenh anthracite coal mine (Van Duc ward), Phao Son kaolin mine (Pha Lai ward), Phuc Son refractory clay (Cong Hoa ward) are similar to the classification results from Landsat 8 OLI multispectral image. This is also consistent with the Hai Duong province mineral distribution map of 1:200,000 scale, which is collected from Information Center for Archives and Geological Journal, General Department of Geology and Minerals of Vietnam, http://idm.gov.vn [30].

In this study, the authors also compared the extraction results of clay minerals containing areas in Chi Linh city and ESRI high spatial resolution images (Table 3).

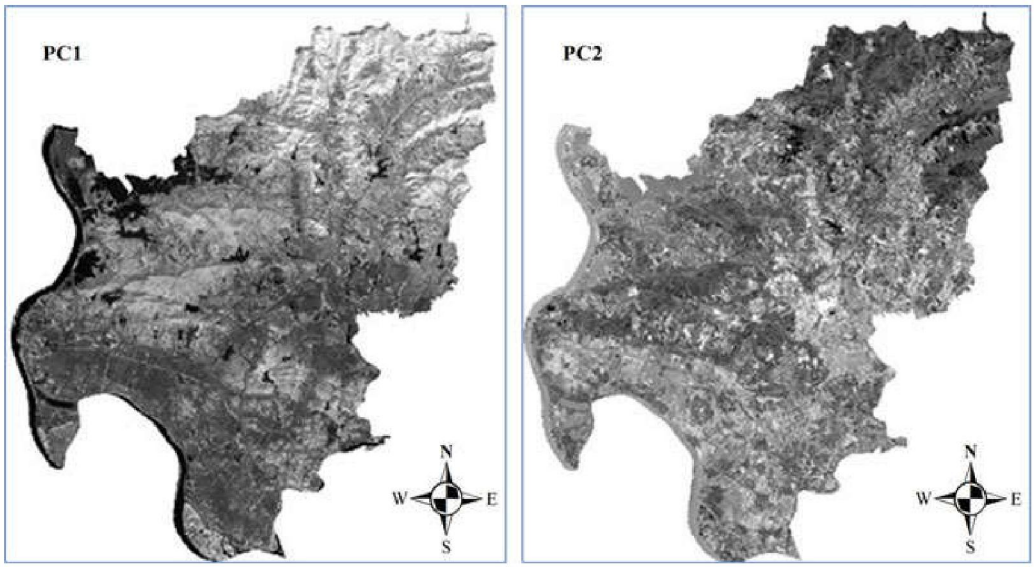

Fig. 9 First and second principal components images

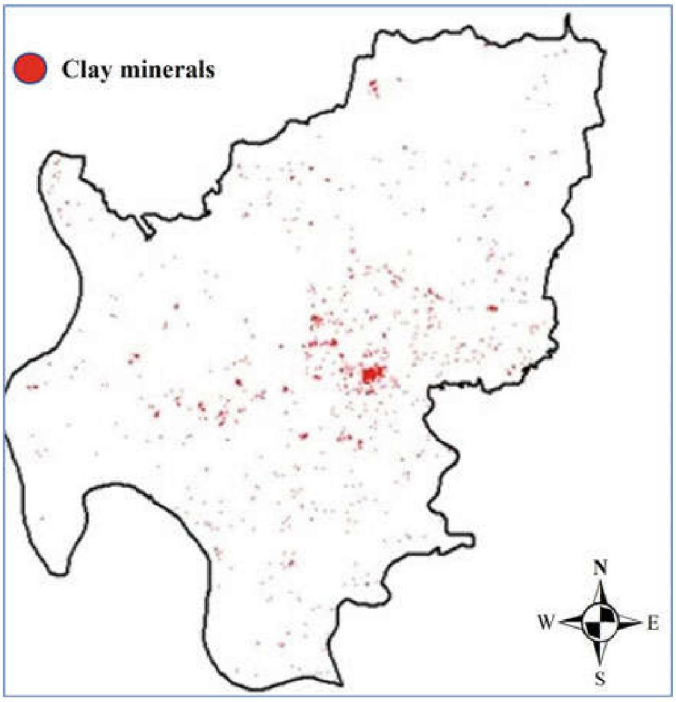

Fig. 10 Result of clay minerals extraction from Landsat 8 data (Chi Linh city, Hai Duong province)

Table 3 shows that, the clay minerals containing areas such as Cong Hoa, Hoang Tien, Van An locations and refractory brick factory have been accurately classified from the Landsat 8 OLI data based on proposed method.

5 Conclusion

This study presents an automatic method solution for clay mineral containing areas extraction from Landsat 8 OLI satellite images on the basis of combining band rationing and principal component analysis method.

Table 3 Compare the classification results of areas containing clay minerals and images from high-resolution satellite images

Position	ESRI high spatial resolution images	Areas containing clay mineral classified from Landsat 8 data
Cong Hoa (Chi Linh city) (21°7′13″N, 106°22′27″E)		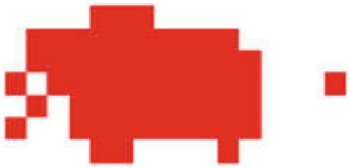
Hoang Tien (Chi Linh city) (21°8′35″N, 106°27′39″E)		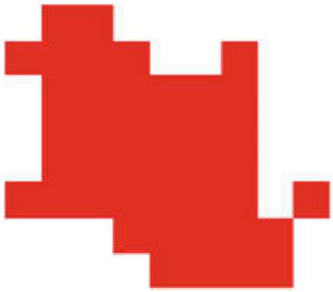
Van An (Chi Linh city) (21°6′37″N, 106°20′46″E)		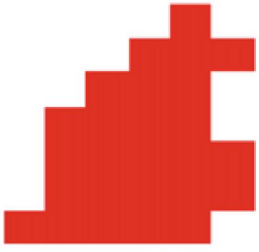

(continued)

Table 3 (continued)

Position	ESRI high spatial resolution images	Areas containing clay mineral classified from Landsat 8 data
Refractory brick factory (21°8′02″N, 106°24′24″E)		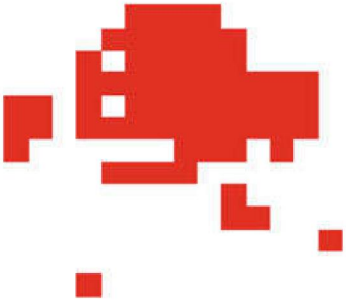

The Landsat 8 OLI image acquired on December 1, 2021 is analyzed to map the spatial distribution of the clay minerals in Chi Linh city, Hai Duong province (northern Vietnam). Four Landsat 8 OLI bands including red (band 4), near-infrared (band 5), and two middle infrared bands (band 6 and band 7) were used to calculate band rationing images, then use principal component analysis method to select the principal component containing a lot of information about clay minerals containing areas. In this study, clay minerals containing areas were extracted based on the automatic thresholding method.

The results obtained in this study show that, Landsat 8 OLI data can be used effectively in extracting and mapping clay minerals containing areas distribution. Along with the successful launch of the Landsat 9 satellite in 2021, the Landsat 8/9 imagery is an effective data source in mineral exploration and discovery.

References

1. Luu, D.-H., Nguyen, T.H.-L.: Renewable energy policies for sustainable development in Vietnam. Vietnam National Univ. J. Sci. Earth Environ. Sci. **25**(3), 133–142 (2009)
2. Vietnam National Coal-Mineral Industries Holding Corporation Limited (Vinacomin). Retrieved from http://www.vinacomin.com.vn
3. Goetz, A.-F., Rock, F.-H., Rowa, B.-N.: Remote sensing for exploration: an overview. Econ. Geol. **78**, 573–590 (1983)
4. Rajesh, H.-M.: Application of remote sensing and GIS in mineral resource mapping–An review. J. Mineral. Petrol. Sci. **99**(3), 83–103 (2004)
5. Abrams, M.-J.: Remote sensing of porphyry copper in Southern Arizona. Econ. Geol. **78**, 591–604 (1983)
6. Abrams, M.-J., Hook, S.-J.: Simulated Aster data for geologic studies. IEEE Trans. Geosci. Remote Sens. **33**, 692–699 (1995)

7. Hu, B., Xu, Y., Wan, B., Wu, X., Yi, G.: Hydrothermally altered mineral mapping using synthetic application of Sentinel-2A MSI, ASTER and Hyperion data in the Duolong area, Tibetan Plateau, China. Ore Geol. Rev. **101**, 384–397 (2018)
8. Roman, A., Ursu, T.: Multispectral satellite imagery and airborne laser scanning techniques for the detection of archaeological vegetation marks. In: Landscape archaeology on the northern frontier of the Roman Enpire at porolissum–an interdiscliplinary research project. Mega Publishing House (2016)
9. Van der Meer, F.D., van der Werff, H.M.A., van Ruitenbeek, F.J.A.: Potential of ESA's Sentinel-2 for geological applications. Remote Sens. Environ. **148**, 124–133 (2014)
10. Alasta, A.-F.: Using remote sensing data to indentify iron deposits in central western Libya. In: International Conference on Emerging trends in Computer and Image processing, Bangkok, 56–61 (2011)
11. Bennett, S.-A., Atkinson, W.-W., Kruse, F.-A.: Use of Thematic Mapper imagery to identify mineralization in the Santa Teresa district, Sonora, Mexico. Int. Geol. Rev. **35**, 1009–1029 (1993)
12. Carranza, E.J.-M., Hale, M.: Mineral imaging with Landsat Thematic Mapper data for hydrothermal alteration mapping in heavily vegetated terrane. Int. J. Remote Sens. **23**, 4827–4852 (2002)
13. Crosta, A.-P., Moore, J.-M.: Enhancement of LANDSAT Thematic Mapper imagery for residual soil mapping in SW Minas Gerais State Brazil: a prospecting case history in greenstone belt terrain. In: Proceedings of the 9th Thematic Conference on Remote Sensing for Exploration Geology, Calgary (Ann Arbor, MI: Environmental Research Institute of Michigan), 1173–1187 (1989)
14. Kaufman, H.: Mineral exploration along the Agaba-Levant structure by use of TM-data concepts, processing and results. Int. J. Remote Sens. **9**, 1630–1658 (1988)
15. Crosta, A.-P., Rabelo, A.: Assessing Landsat TM for hydrothermal mapping in central-western Brazil. In: Proceedings of the Ninth Thematic Conference on Geologic Remote Sensing, Pasadena, California, USA, 1053–1061 (1993)
16. Mia, M.-B., Fujimitsu, Y.: Mapping hydrothermal altered mineral deposits using LANDSAT 7 ETM+ image in and around Kuju volcano, Kyushu, Japan. J. Earth Syst. Sci. **121**(4), 1049–1057 (2012)
17. Pour, A.-B., Hashim, M.: Integrating PALSAR and ASTER data for mineral deposits exploration in tropical environments: a case study from Central Belt, Peninsular Malaysia. Int. J. Image Data Fusion **6**(2), 170–188 (2015)
18. Fraster, S.-J., Green, A.-A.: A software defoliant for geological analysis of band ratio. Int. J. Remote Sens. **8**, 525–532 (1987)
19. Trinh, L.H., Zablotskii, V.R.: The method of detection of clay minerals and iron oxide based on Landsat multispectral images (as exemplified in the territory of Thai Nguyen province, Vietnam). Min. Sci. Technol. **4**(1), 65–75 (2019)
20. Trinh, L.H., Nguyen, V.N.: Mapping coal files using Normalized Difference Coal Fire Index (NDCfI): case study at Khanh Hoa coai mine, Vietnam. Min. Sci. Technol. **6**(4), 233–240 (2021)
21. Trinh, L.H.: Application of band ratio method to detect iron oxide, clay minerals and ferrous minerals. Min. Ind. J. **4**, 19–24 (2013)
22. Electronic portal of Chi Linh city. Retrieved from https://chilinh.haiduong.gov.vn/
23. National Aeronautics and Space Administration. Retrieved from https://landsat.gsfc.nasa.gov/satellites/
24. United States Geological Survey. Retrieved from https://glovis.usgs.gov
25. Clark, R.-N., Swayze, G.-A., Wise, R., Livo, K.-E., Hoefen, T.-M., Kokaly, R.-F., Sutley, S.-J.: USGS digital spectral library. USGS Open File Rep (1989)
26. Hunt, G.-R., Ashley, R.-P.: Spectra of altered rocks in the visible and near infrared. Econ. Geol. **74**, 1613–1629 (1979)
27. Clark, R.-N.: Spectroscopy of rock and minerals and principles of spectroscopy. In: Rencz, A.-N. (ed.) Remote Sensing for the Earth Sciences, Manual of Remote Sensing 3, pp. 3–58. Wiley, New York (1999)

28. Mohamed, E.-S., Saleh, A.-M., Belal, A.-B., Gad, Abd. -A.: Application of near-infrared reflectance for quantitative assessment of soil properties. Egypt. J. Remote Sens. Space Sci. **21**(1), 1–14 (2018)
29. Loughlin, W.-P.: Principal component analysis for alteration mapping. Photogram. Eng. Remote Sens. **57**(g), 1163–1169 (1991)
30. Inf. Cent Arch. Geol. J. General Department of Geology and Minerals of Vietnam. Retrieved from http://idm.gov.vn